Design of Attitude Control System for Dragonfly-Inspired Flapping Wing Aerial Vehicle

Lei Wang[1], Xiaojun Yang[1,2,3] , Yang Luo[1], Hang Chen[1]& Junying Li[1]

[1] School of Aeronautics, Northwestern Polytechnical University, Xi'an, Shaanxi 710072, China;
[2] National Key Laboratory of Aircraft Configuration Design, Xi'an, Shaanxi 710072, China;
[3] Research & Development Institute of Northwestern Polytechnical University in Shenzhen, Shenzhen, Guangdong, 518057, China.

Abstract

For general insect like tailless flapping wing aerial vehicle(FWAV), relying solely on the flapping motion of the wings should generate both lift and control torque. Due to the inherent instability of tailless FWAV, a wing control mechanism is needed to generate effective control torque to stabilize the aircraft. This article introduces a control system applied to a 65g level dragonfly-Inspired FWAV, which can control pitch, roll, and yaw by changing the flapping frequency and the flapping plane angles of its two wings, so as to maintain a stable attitude of the aircraft during hovering. We first designed a compact and lightweight flapping mechanism, and then determined through force measurement and pole climbing experiments that it can generate sufficient lift. Subsequently, a control mechanism was designed to control the flapping plane angles. Single degree of freedom and three degree of freedom bench experiments were conducted to verify the effectiveness of the attitude control system.

Keywords: Flapping wing aerial vehicle, Flapping-wing mechanism, Attitude control system, Bench test

1. General Introduction

The flight mechanisms of avian and insect species in nature have perennially captivated human fascination and inspired emulation in the realm of aerial vehicle design. With the current advancements in microelectronics, micro-mechanical systems and nonlinear control technologies, the challenges that once hindered the theoretical and engineering research of biomimetic FWAVs have been significantly mitigated. These developments have catalyzed FWAVs into becoming a prominent research topic globally. Compared to conventional rotorcraft and fixed-wing aircraft, FWAVs offer salient benefits, including reduced size and weight, enhanced flight efficiency[1,2], superior concealment, and augmented maneuverability[3]. Specifically, the dragonfly, an adept flyer within the insect kingdom, achieves remarkable maneuverability and complex flight patterns through the independent control of its two pairs of wings. Leveraging these unique advantages, the dragonfly-inspired FWAVs play an irreplaceable role in special military and civilian fields where high demands are placed on stealth and maneuverability.

For micro flapping wing aerial vehicles, compared with traditional aircraft or large flapping wing vehicles, the design of their attitude control system presents more challenges. Due to their smaller inertial and mass properties, micro FWAVs are more susceptible to external perturbations such as aerodynamic forces and wing-induced disturbances, significantly influencing vehicular stability. Moreover, their response to control inputs is faster, demanding higher sensitivity from the control system. Additionally, due to the reduced scale of the vehicles, higher requirements are placed on the size and precision of sensors and control systems. Even minor sensor errors or inaccuracies in the control system can cause the vehicle to deviate from its stable attitude. After a series of design and research on the aerodynamic performance and micro driving mechanism of the serial flapping wing, we further designed the attitude control system of the dragonfly-Inspired prototype and verified the final attitude control effect of the prototype on the bench setup.

2. Flapping-wing mechanism

2.1 Conceptual design and fabrication

According to the previous research of our team on flapping wing design[4], the designed flapping frequency of the flapping wing used in this prototype is around 20Hz, with a flapping amplitude of 120 °, and the flapping law is close to a sinusoidal pattern. The papers should be prepared, if possible, using the format like this document. According to the previous research on flapping wing design, the designed flapping frequency of the flapping wing used in this prototype is around 20Hz, with a flapping amplitude of 120 °, and the flapping law is close to a sinusoidal law. Under the design requirements of small-sized driving mechanisms, compared to crank slider mechanisms and spatial linkage mechanisms, planar linkage mechanisms have a simple form, high reliability, and are easy to maintain. After considering the processing technology and reliability, this article ultimately chose the composite single crank double rocker mechanism as the flapping mechanism form of the driving unit. Compared with the single-stage crank rocker mechanism, the mechanism selected in this article can improve the quick return characteristics of the mechanism's motion. Figure1(a) is a schematic diagram of the motion of the flapping mechanism. The composite single crank double rocker mechanism can be regarded as a planar six bar mechanism, consisting of a first stage crank rocker mechanism and a second stage double rocker mechanism, respectively. The crank a1 in the first stage mechanism drives the rocker c1 of the first stage mechanism to swing with an output angle of Φ1 through turnover motion. The second stage is a double rocker mechanism, as shown in Figure1(b). The rocker c1 of the first stage mechanism is fixedly connected to the a2 of the second stage mechanism, and the angle between c1 and a2 is γ. The output angle(Φ1) of c1 is converted into the input angle(θ2) of the second stage joystick a2, and then the input angle(θ2) is converted into the swinging motion of the second stage joystick c2 with an angle of Φ2. In order to reduce the overall size of the mechanism, the second-stage mechanism is arranged with installation angles Λ1 and Λ2.

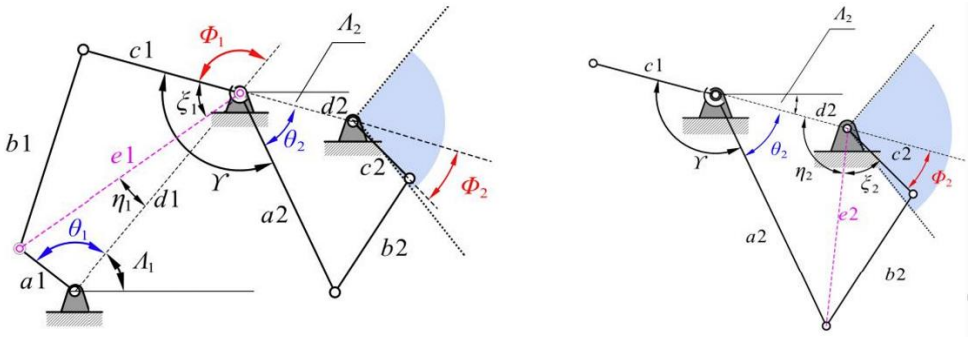

Figure 1(a) – the motion of the flapping mechanism. Figure 1(b) – double rocker mechanism.

To optimize the design of the flapping mechanism, it is first necessary to establish kinematic equations and solve the relationship between input and output. Based on the knowledge of mechanical principles, the following kinematic equations can be obtained for the planar six bar mechanism shown in the figure 1:

$$\begin{cases} e_1^{\,2} = a_1^{\,2} + d_1^{\,2} - 2a_1 d_1 \cos\theta_1 \\ \eta_1 = \arccos\left(\dfrac{e_1^{\,2} + d_1^{\,2} - a_1^{\,2}}{2e_1 d_1} \right) \\ \zeta_1 = \arccos\left(\dfrac{e_1^{\,2} + c_1^{\,2} - b_1^{\,2}}{2e_1 c_1} \right) \\ \phi_1 = \pi - \eta_1 - \zeta_1 \\ \theta_2 = 2\pi - \phi_1 - \alpha - \beta - \Upsilon \\ e_2^{\,2} = a_2^{\,2} + d_2^{\,2} - 2a_2 d_2 \cos\theta_2 \\ \eta_2 = \arccos\left(\dfrac{e_2^{\,2} + d_2^{\,2} - a_2^{\,2}}{2e_2 d_2} \right) \\ \zeta_2 = \arccos\left(\dfrac{e_2^{\,2} + c_2^{\,2} - b_2^{\,2}}{2e_2 c_2} \right) \\ \phi_2 = \pi - \eta_2 - \zeta_2 \end{cases} \tag{2-1}$$

After establishing the kinematic equations, then begin to establish optimized boundary conditions. In the first stage crank rocker mechanism, crank a1 is fixedly connected to the reduction gear. Due to the size of the reduction gear and the installation position of crank a1, a1 is set as the given value in the optimization design, and optimization variables b1, c1, and d1 are selected. At the same time, in order to reduce the overall size of the mechanism, when designing the frame d1, the installation angle Λ1 is given as 50 °. The constraint conditions of the first stage mechanism include: satisfying the rod length conditions of the crank rocker mechanism, that is, the sum of the longest and shortest rods is less than or equal to the sum of the other two rods, and the crank is the shortest rod. In this section, take frame d1 as the longest rod and crank a1 as the shortest rod, with the following rod length conditions:

$$\begin{cases} a_1 \le b_1, a_1 \le c_1, a_1 \le d_1 \\ b_1 \le d_1, c_1 \le d_1 \\ a_1 + d_1 \le b_1 + c_1 \end{cases} \tag{2-2}$$

At the same time, in order for the first stage crank rocker mechanism to have a better transmission performance during operation, the following transmission angle conditions also need to be satisfied:

$$\begin{cases} \gamma_1 = \arccos\left(\dfrac{b_1^{\,2} + c_1^{\,2} - (d_1 - a_1)^2}{2b_1 c_1}\right) \ge 45° \\ \gamma_2 = \arccos\left(\dfrac{b_1^{\,2} + c_1^{\,2} - (d_1 + a_1)^2}{2b_1 c_1}\right) \le 135° \end{cases} \tag{2-3}$$

In the second-stage double rocker mechanism, also to control the overall size of the mechanism, the frame length d2, the mounting angle Λ2, and the pinch angle Υ were set to known values, where Λ2 = 10° and Υ = 110°. The design variables are b2, c2, and d2, and during the optimization process, the difference between the maximum and minimum values of the output angle Φ2 of the first-stage mechanism is set to be 120°, and there is no obvious sharp return characteristic in the flutter stroke. The sinusoidal shape function is chosen as the final angular output objective, and the complete flapping of the mechanism in one cycle is discretized into 50 instantaneous positions. the optimization objective of the second-stage mechanism is established as:

$$\min\ f_2 = \sum_1^n \left(\phi_{2i} - \phi_{2E}\right)^2 \tag{3-4}$$

Where Φ_{2i} is the instantaneous output angle of the second-stage mechanism, and Φ_{2E} is the desired output angle. In this section, the desired output angle is set as a trigonometric function law with the

same phase and amplitude as Φ2, and the specific form of Φ_{2E} can be obtained by solving for the output angle Φ2 in the optimization process.

The constraints of the second-level mechanism include: the conditions that constitute the existence of the double rocker mechanism(the sum of the longest rod and the shortest rod is greater than the sum of the other two rods), and setting c2 as the shortest rod, the following constraints are available:

$$\begin{cases} c_2 \le a_2, c_2 \le b_2, c_2 \le d_2 \\ b_2 + d_2 \le a_2 + c_2 \end{cases} \tag{2-5}$$

In order for the mechanism to have a good transmission performance during operation, the following transmission angle conditions also need to be met:

$$\gamma_3 = 180° - \arccos\left(\frac{b_2^{\,2} + c_2^{\,2} - e_2^{\,2}}{2b_2c_2}\right) \ge 45° \tag{2-6}$$

The mechanism output angle Φ2 is also required to satisfy the output angle condition:

$$\max(\phi_2) - \min(\phi_2) = 120° \tag{2-7}$$

Taking Eq. (2-4) as the optimization objective, Eqs. (2-1)~(2-3), (2-5)~(2-7) as the constrained boundary conditions, and setting the convergence tolerance as 1×10^{-8} and the maximum number of iterative steps as 40,000, the length of each stage of the rod and the output angle Φ2 can be obtained. The length of each stage of the rod obtained by optimization is shown in Table 1. From the Figure 2, it can be seen that after optimization, the final output angle law is basically consistent with the trigonometric function law, meanwhile, the output angle range is 120°.

Table 1 – The length of each stage of the rod.

a_1	b_1	c_1	d_1	a_2	b_2	c_2	d_2
5	18.6	10.7	21.4	15	9.5	8.5	9.75

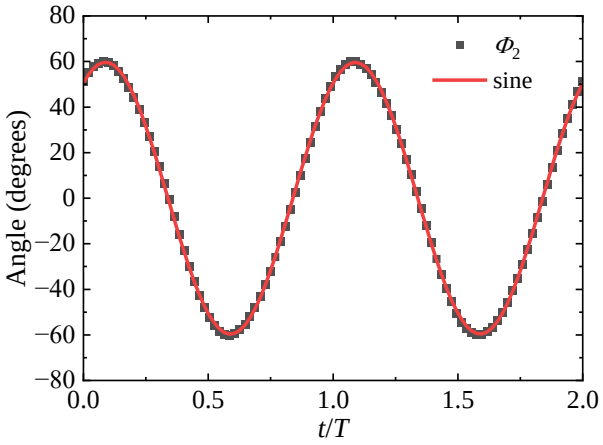

Figure 2 – The final output angle law.

In the arrangement of the mechanism, compared with the single-layer mechanism arrangement, take the form of multi-layer mechanism arrangement, is conducive to saving space and constraints on the movement of parts. In the selection of materials for each component, the upper and lower frame and the second stage connecting rod of the mechanism use carbon fiber plate, the quality of carbon fiber plate is easier to process, while the strength performance is excellent; the rest of the key drive mechanism components are processed with aluminum alloy; for the irregularly shaped motor support and some of the buckles, 3D printing is used to make the material of resin or nylon. The gear reducer is a two-stage gear reduction design, the gear is made of aluminum alloy, and the motor gear is brass. In the transmission mechanism, bearings are added at each rotating part to reduce friction.

The final formation of the flapping mechanism is shown in the Figure 3, with a wingspan of 29cm.

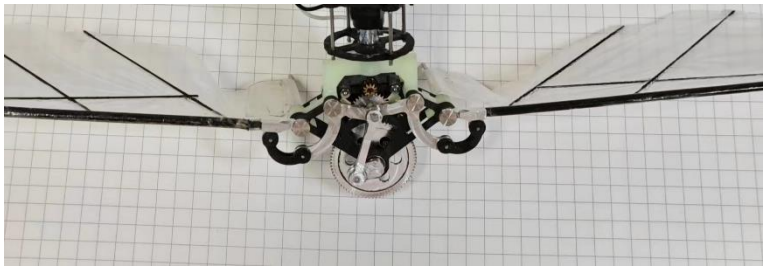

Figure 3 – The final formation of the flapping mechanism.

2.2 Lift test

After completing the design and fabrication of the flutter mechanism, we carried out the tandem wing lift test and pole-climbing experiment. As shown in Figure 4, a pair of flapping mechanism is fixed symmetrically on both sides of the load cell, and an external power supply is used to supply power to the motors ,then test the lift of the tandem wing under different duty cycles respectively.

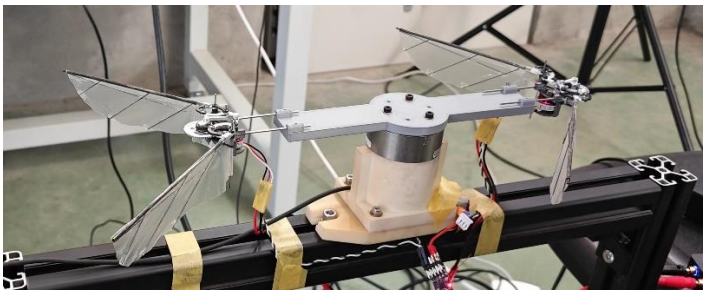

Figure 4 – load cell setup.

Figure 5 shows the change curve of instantaneous lift in 1s under 0.5 duty cycle, and it can be seen that the instantaneous lift is cyclic, with about 14 cycles, i.e., the frequency of the flutter is 14hz, and the lift in each cycle shows two peaks in the shape of the waveform, and the dotted line is the average lift at 0.5 duty cycle, which is about 53 g. The statistics of the average lift at different duty cycles are shown in Figure 6. The lift at 0.7 duty cycle is about 100 g, which is larger than the estimated weight of the prototype (65 g), and there is enough maneuvering torque left.

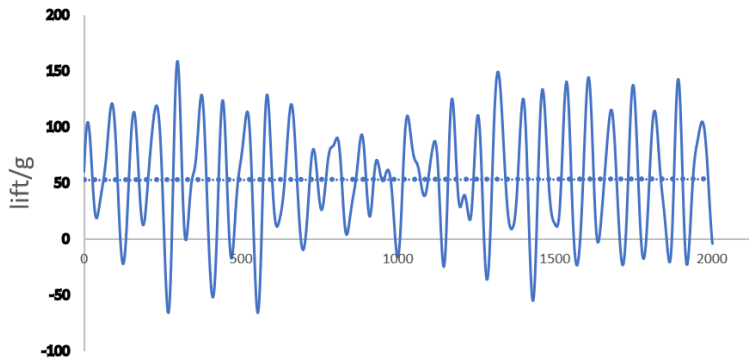

Figure 5 – The instantaneous lift in 1s under 0.5 duty cycle.

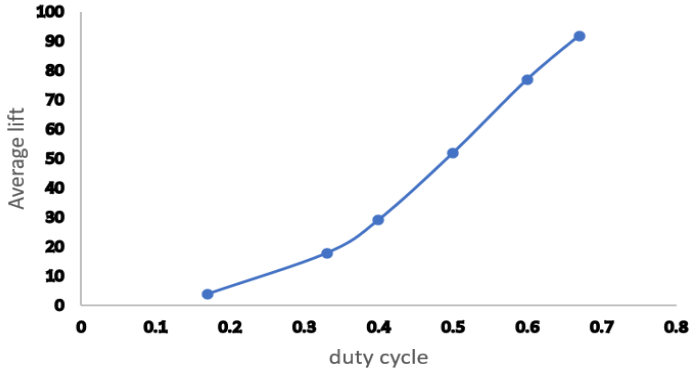

Figure 6 – The instantaneous lift in 1s under 0.5 duty cycle.

The prototype of the first remote control was then assembled and pole-climbing experiments were conducted. Two guide rods were set up and fixed at the top and bottom, while linear bearings that could rise along the guide rods were installed on the prototype. When the throttle was pushed, it was observed whether the prototype could generate enough lift to rise along the guide rods and could hover at a certain position on the guide rods.

At the beginning of the experiment, the climbing situation of the prototype was recorded by video camera. The experimental results are shown in Figure 7. It can be seen that during the experiment, the prototype has an obvious climbing action, starting from the moment of t=0.25s. until it reaches the highest point at the moment of t=2.25s. After that, it maintains the hovering state, which proves the effectiveness of the flapping mechanism.

t=0.25s t=1s t=1. 5s t=2.25s

Figure 7 – The pole-climbing experiments.

3. Attitude control mechanism

The design of the attitude control system for FWAVs initially requires the formulation of attitude control strategies. For the control strategies of FWAVs, researchers both domestically and internationally have embarked on relevant explorations, with control strategies of some typical FWAVs summarized in Table 2. Given the limitations posed by the existing drive technology, the weight of the prototype, and the complexity of the prototype, it is necessary to comprehensively select the control degrees of freedom for the biomimetic flapping wing vehicle, considering the provided control torque.

As shown in Table 2, the way of generating control torque for the insect-like flapping wing vehicle mainly comes from the change of the relevant motion parameters of the flapping wing, which mainly include the flapping frequency, the flapping amplitude, the mid-stroke angle (the offset angle of the flapping centerline of a pair of flapping wings with respect to the axis of the fuselage), the flapping twist angle, the stroke plane angle, and the flapping rotation angle. By combining these motion parameters, a reasonable attitude control mode can be obtained in a certain state. The effects of these combinations of motion parameters are reflected in the overall motion of the flapping wing, which can be categorized into the following modes:

Wing Twist Modulation.

Wing Rotation Modulation: Including active control of flapping rotation angle, control of split cycle

parameter.

Flapping Plane Tilting.

Flapping Frequency, Amplitude and Offset Modulation.

Variable flapping amplitude and mid-stroke angle are generally realized by complex mechanical structure or direct-drive system; the flapping rotation angle is generally modulated by direct-drive system, and can also be realized by rope or lever system; variable flapping twist angle and flapping frequency can be realized directly by servo and motor; variable stroke plane angle control is more direct, does not need complex mechanical structure and does not produce lift loss, and the wing can be designed to maintain the optimal motion at all times, but it requires more load capacity for the servo.

Table 2 – Control strategies of some typical FWAVs

Name	Weight（g）	Wing Span（cm）	Flapping frequency（Hz）	Control strategies
Festo BionicOpter	175	63	15-20	Four-wing independent control of wing flapping amplitude and rotation angle[5].
DElFLY Nimble	28.2	33	17	Pitch: mid-stroke angle Roll: flapping frequency Yaw: flapping twist angle [6]
Robotic Hummingbird	64	30.5	22	Pitch, Yaw：Stroke plane angle Roll：flapping amplitude[7]
QV	25	15	39	Four-wing independent control of wing flapping amplitude[8]
Nano hummingbird	19	16.5	30	Pitch, Roll：flapping twist angle Yaw：flapping rotation angle[9]
Kubeetle	16.4	17	23	Pitch, Roll, Yaw：flapping twist angle[10]
Deng. hummingbird	12	17	34	Pitch: mid-stroke angle Roll: flapping amplitude Yaw: split cycle parameter [11]
Robobee	0.08	3.5	120	Pitch: mid-stroke angle Roll: flapping amplitude Yaw: split cycle parameter [12]

The definition of the aircraft rotation axis system is shown in Figure 8. Rotation around the x-axis is defined as the aircraft's rolling motion, rotation around the y-axis is defined as the aircraft's pitch motion, and rotation around the z-axis is defined as the aircraft's yaw motion. For this prototype, the control torque generated by changing different motion parameters is shown in Figure 9. Since the flapping mechanism designed in this paper is more compact and lighter in weight, and motors are used to control the two pairs of wings separately, in summary, the prototype in this paper will be controlled based on the flapping frequency and the stroke plane angle. For the flapping plane tilt

structure, the form of cantilever beam is used to directly connect the flapping mechanism with the servo output shaft, which is simple and reliable, but puts forward high requirements for the performance of the servo. The servo used weighs about 2.8g, and under the 5v energization, the torque is 0.72Kgf.cm, and the speed is 0.049sec/60°.

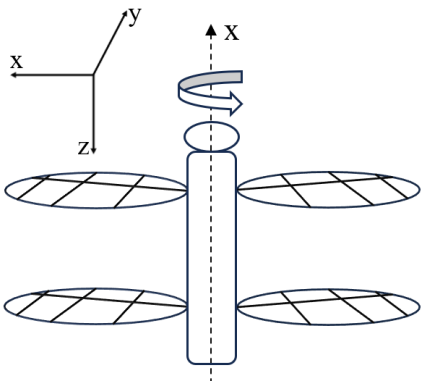

Figure 8 – The definition of the aircraft rotation axis system.

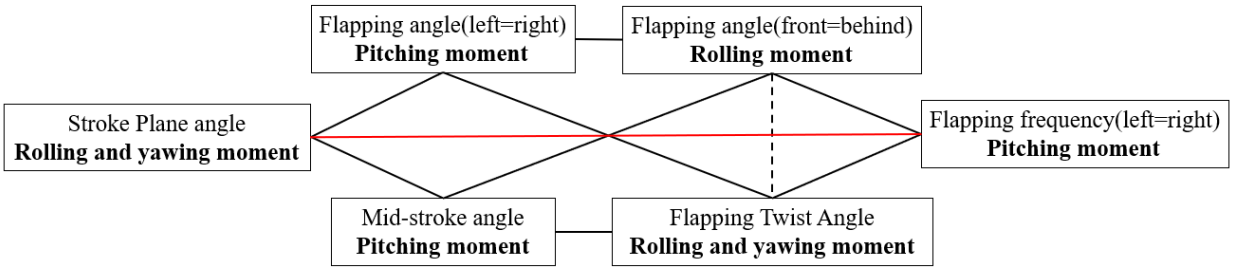

Figure 9 – The control torque generated by changing different motion parameters.

As shown in the Figure 10, the red arrows represent the lift vectors, the roll moment is generated when the two pairs of wing's stroke planes are rotating in the same direction, the yaw moment is generated when the two pairs of wing's stroke planes are rotating in the opposite direction, and the pitching moment is generated by the difference of the two pairs of wing's flapping frequency.

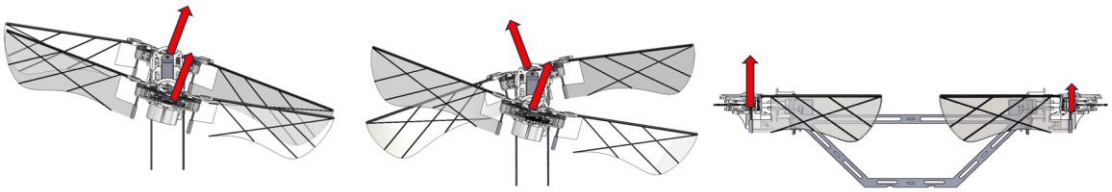

Figure 10 – The control torque generated by changing different motion parameters.

4. Attitude stabilization

4.1 Avionics

The requirements for the flight control hardware solution of the micro FWAV are mainly focused on low power consumption, light weight, small size, sensor accuracy and chip computing power. According to the above requirements, the team selected the Omnibus open source hardware program and Pixracer open source hardware program as the reference program for the development of flight control hardware for the prototype. Based on these two solutions, the FN22 flight control board was developed by removing redundant functions, streamlining the device volume and space, and optimizing the alignment arrangement. The weight of the flight control board is 2.2g, the size is 20*23mm, the power consumption is 0.8W, equipped with STM32F4 chip, Invensense MPU-9250 three-axis accelerometer and gyroscope. In addition, ST LIS3MDL magnetometer sensor and MEAS MS5611 barometer sensor are added to further broaden the use of the flight control scene. The flight control chip is designed with a corresponding TF memory card slot, and equipped with a complete digital transmission link and interface, so it has a complete log storage and ground station communication function. As for the receiver, the receiver uses S-FHSS as the wireless transmission protocol, and communicates with the flight control using the SBUS/PPM protocol. In addition, I2C, SPI and UART interfaces have been added for external sensors such as magnetometers and navigation modules.

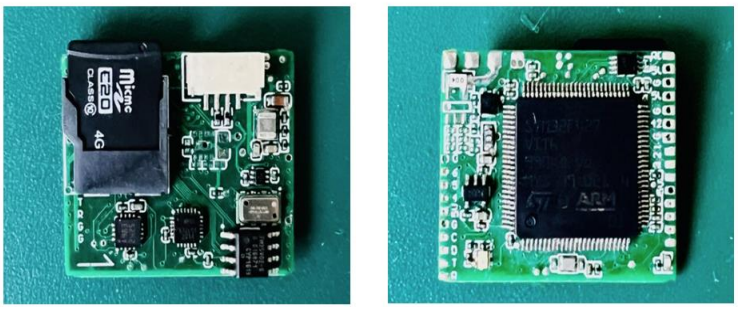

Figure 11 – The FN22 flight control board.

Due to the inherent instability of a tailless FWAV, an angular-angular velocity cascade PID controller is used in the control system to control the attitude of the vehicle. The cascade PID control usually consists of two PID controllers: an outer PID controller and an inner PID controller. The outer PID controller receives the error signal between the desired and actual outputs of the system and produces a control output that is used to control the setpoint of the inner PID controller. The inner PID controller receives the output of the outer PID controller as its setpoint and controls the actual process variables of the system. For the pitch and roll angle attitude control system, as shown in the Figure 12, the outer layer is the angle layer, the desired attitude angle of the outer layer and the actual attitude angle difference to get the attitude angle error, the angle error will be input into the p-controller, the output value is the set angular rate, the set angular rate and the actual angular velocity difference to get the angular rate error, input the rate error into the PD+F controller, the output value is the control quantity, the control quantity will be allocated by mixing control to get the actual PWM value of the actual actuator. Attitude control of yaw angle takes only a single stage of angular rate PD+F control.

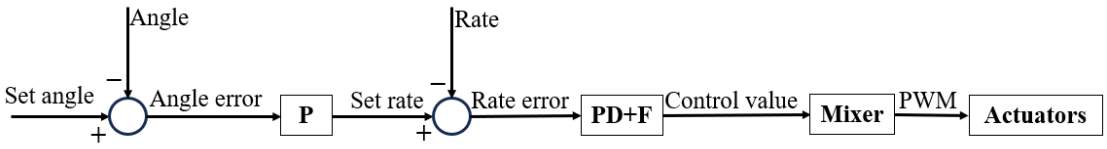

Figure 12 – The angular-angular velocity cascade PID controller.

4.2 Bench Test

After completing the prototype production and avionics integration, in order to verify the feasibility of the control strategy and control system, two small bench test setups were made, which were roll, pitch single degree of freedom bench experiment and roll pitch yaw three degrees of freedom bench experiment respectively, the three degrees of freedom bench has a very light weight, which can be as close as possible to the rotational inertia of the original aircraft. The flight log is recorded by on-board sd card to read the attitude angle information of the prototype; and the prototype is recorded by high-speed video camera to observe the flight attitude response and make parameter adjustments.

For the roll angle single-degree-of-freedom experiment, as shown in the Figure 13, install the roll sleeve on the fuselage, the installation position and the center of gravity of the fuselage is at the same height, and then install the prototype on the roll shaft, switch the prototype to self-stabilizing mode, support the prototype during takeoff, push the throttle stick to 70% and then let go, and observe whether the aircraft can maintain a stable attitude.

By reading the log message, it can be seen that the roll angle error is stabilized at about +-2°, which has a good control effect; the same single-degree-of-freedom experiment is conducted for pitch angle, and it can be seen that the pitch angle is stabilized at about +6~-4°; finally, the three-degree-of-freedom experiment is conducted for the bench test, and it can be seen that the three-axis attitude angle is stabilized at less than 6°. Through the bench experiment, it is determined that the attitude control strategy of the prototype is feasible, and the attitude control algorithm is robust enough to realize the stable control of the prototype's attitude under high-frequency flapping.

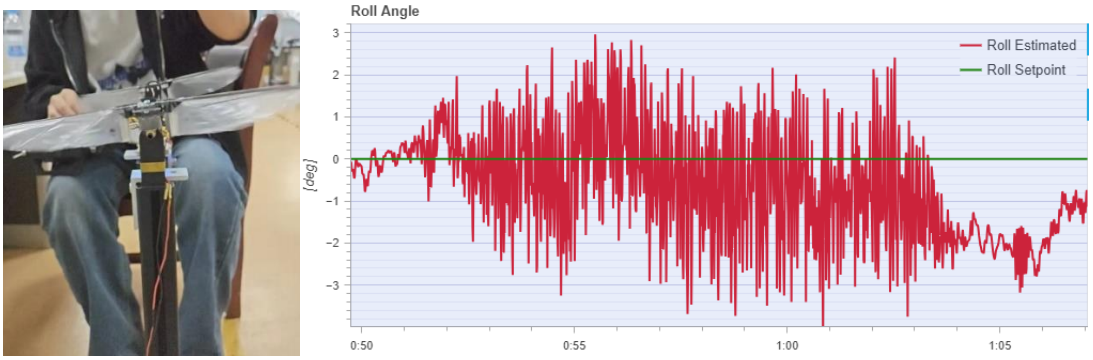

Figure 13 – The roll angle single-degree-of-freedom experiment.

Figure 14 – The pitch angle single-degree-of-freedom experiment.

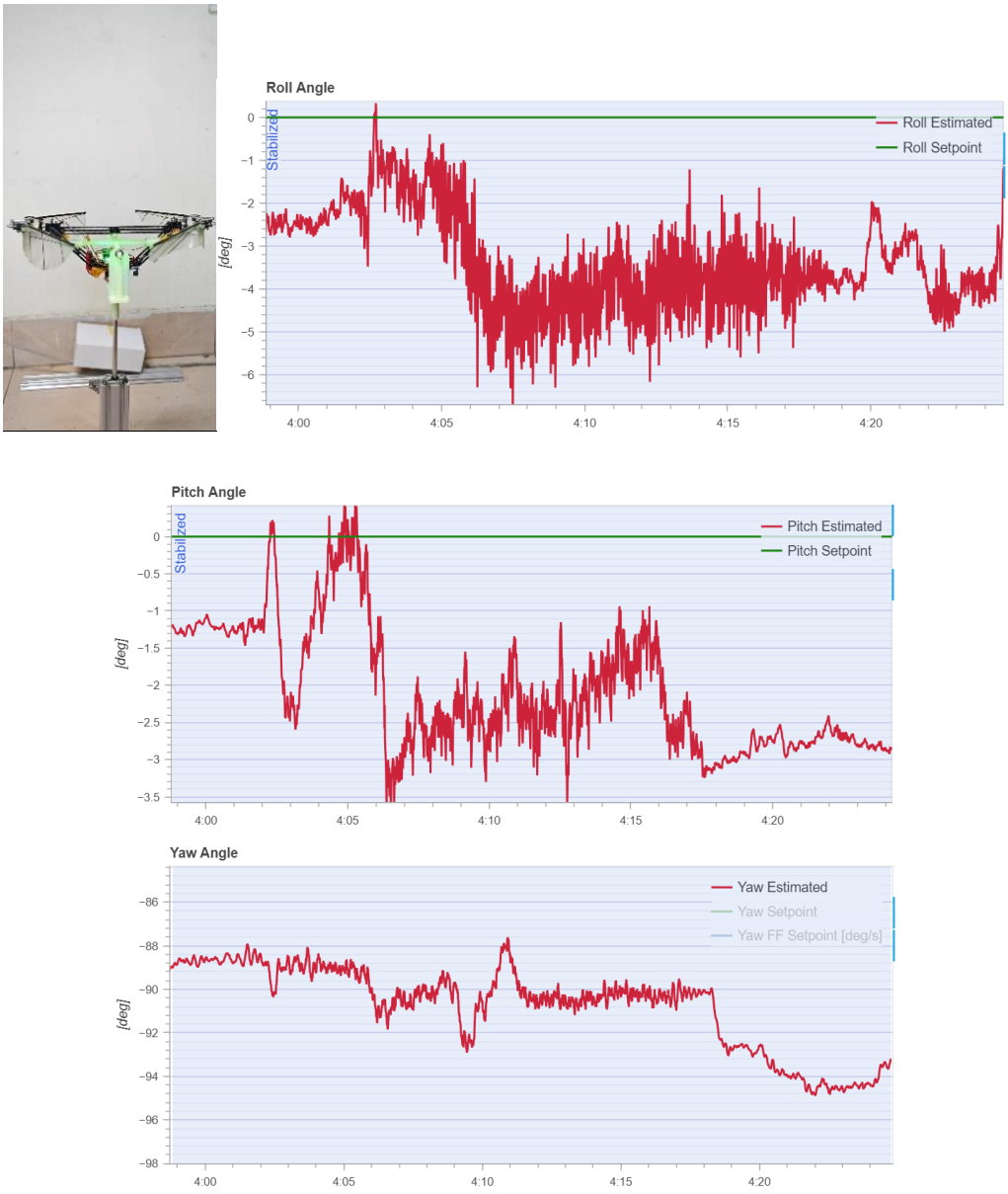

Figure 15 – The three-degree-of-freedom experiment.

5. Conclusion

This paper presents the design process of the control system of a tailless dragonfly-inspired FWAV with a weight of 65g and a wingspan of 29cm, which can control pitch, roll and yaw by changing the flapping frequency as well as the stroke plane angles of its two pairs of wings. The proposed flapping mechanism is compact and light; the control mechanism, with a simple structure, is easy to be assembled and has a lighter weight compared with the control mechanism of the same type of vehicle. Through the load cell experiment and pole-climbing experiment, it is proved that the flapping mechanism can generate enough lift force and leave maneuvering margin; through the bench experiment, it is proved that the control mechanism can effectively generate control torque and maintain attitude stability. The design and validation of the attitude control system of this dragonfly-inspired FWAV is successfully completed.

6. Contact Author Email Address

The contact author email address: xjyang518@nwpu.edu.cn

7. Acknowledgments

This work is financially supported by the Shenzhen Science and Technology Program and Research under Grant No. JCYJ20220530161808018, and Guangdong Basic and Applied Basic Research Foundation under Grant No. 2023A1515010776. Key R&D Program in Shaanxi Province of China

under Grant No. 2023-YBGY-372.

8. Copyright Statement

References

[1] Shyy W, Aono H, Chimakurthi S K, et al. Recent progress in flapping wing aerodynamics and aeroelasticity[J]. Progress in Aerospace Sciences, 2010, 46(7): 284–327.

[2] Pesavento U, Wang Z J. Flapping wing flight can save aerodynamic power compared to steady flight[J]. Physical Review Letters, 2009, 103(11).

[3] Shyy W, Berg M, Ljungqvist D. Flapping and flexible wings for biological and micro air vehicles[J]. Progress in Aerospace Sciences, 1999, 35(5): 455–505.

[4] Lang, X.; Song, B.; Yang, W.; Yang, X.; Xue, D. Sensitivity Analysis of Wing Geometric and Kinematic Parameters for the Aerodynamic Performance of Hovering Flapping Wing. Aerospace 2023, 10, 74.

[5] Nina Gaissert, Rainer Mugrauer, Günter Mugrauer, Agalya Jebens, Kristof Jebens, and Elias Maria Knubben. Inventing a Micro Aerial Vehicle Inspired by the Mechanics of Dragonfly Flight.

[6] Matej Karásek, Florian T. Muijres, Christophe De Wagter, Bart D. W. Remes and Guido C. H. E. de Croon. A tailless aerial robotic flapper reveals that flies use torque coupling in rapid banked turns. Science 361 (6407), 1089-1094. DOI: 10.1126/science.aat0350.

[7] David Coleman, Moble Benedict, Vikram Hrishikeshavan, Inderjit Chopra. Design, Development and Flight-Testing of a Robotic Hummingbird. May 2015. Conference: American Helicopter Society 71st Annual ForumAt: Virginia Beach, VA

[8] Jayant Ratti · George Vachtsevanos. Inventing a Biologically Inspired, Energy Efficient Micro Aerial Vehicle. J Intell Robot Syst (2012) 65:437–455,DOI10.1007/s10846-011-9615-z.

[9] Matthew Keennon, Karl Klingebiel, Henry Won, and Alexander Andriukov4 AeroVironment Inc., Simi Valley, CA, 93065. Development of the Nano Hummingbird: A Tailless Flapping Wing Micro Air Vehicle. AIAA 2012-0588.

[10] Phan HV, Aurecianus S, Kang T, Park HC. KUBeetle-S: An insect-like, tailless, hover-capable robot that can fly with a low-torque control mechanism. International Journal of Micro Air Vehicles. 2019;11. doi:10.1177/1756829319861371

[11] Jian Zhang, Zhan Tu, Fan Fei, and Xinyan Deng. Geometric Flight Control of a Hovering Robotic Hummingbird. 2017 IEEE International Conference on Robotics and Automation (ICRA) Singapore, May 29 - June 3, 2017

[12] Kevin Y. Ma, Pakpong Chirarattananon, Sawyer B. Fuller, and Robert J. Wood. Controlled Flight of a Biologically Inspired, Insect-Scale Robot. Science 340 (6132), . DOI: 10.1126/science.1231806.